JOC Article
pubs.acs.org/joc

Mechanism and Stereoselection in a Y-Catalyzed Transacylation Reaction. A Computational Modeling Study

Toby T. Sanan, T. V. RajanBabu,* and Christopher M. Hadad*

Department of Chemistry, 100 West 18th Avenue, Ohio State University, Columbus, Ohio 43210

rajanbabu.1@osu.edu; hadad.1@osu.edu

Received February 5, 2010

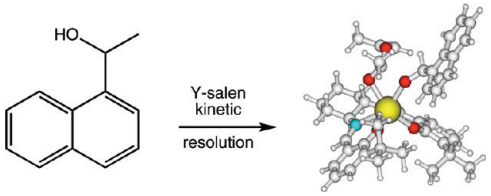

Density functional theory calculations were performed to evaluate the proposed mechanism of a yttrium−salen complex-catalyzed acylation of secondary alcohols using an enol acetate as the acyl-transfer agent. A key step in the proposed mechanism is an intramolecular nucleophilic reaction between the coordinated alcohol and enol ester, brought into close proximity by the yttrium catalyst. The use of the BP86 pure density functional for reproduction of the geometry of the yttrium complex was validated by comparison with the experimental crystal structure. Mapping of the free energy surface of the reaction followed, employing both the BP86 and B3LYP functionals, and results suggest that the proposed mechanism (*Org. Lett.* **2002**, *4*, 1607−1610) is a reasonable pathway for the reaction. Reproduction of the experimentally observed enantioselectivity of the reaction was subsequently attempted, with diastereomeric transition states identified for the turnover-limiting step in the reaction, the intramolecular nucleophilic attack of the alcohol into the enol ester reagent. The predicted experimental enantioselectivities were successfully reproduced for the three ligands studied, although the energetic predictions did not perfectly correlate with the experimental enantioselectivities.

Introduction

Esters are ubiquitous compounds in organic chemistry, used both as protecting groups and as key intermediates in functional group transformations. New highly efficient and selective methods for the synthesis of these compounds continue to evolve. In this context, two of the most significant recent advances have been in the use of better acyl transfer agent/catalyst combinations[1a,b] and the discovery of new protocols for kinetic resolution of secondary alcohols.[1c−g] Enol esters as sources of irreversible acyl transfer agents have been used in enzymatic[2a−c] and nonenzymatic[2d,e] reactions. Searching for a metal-mediated acyl transfer reaction, RajanBabu and co-workers found that primary and secondary alcohols react with enol esters at room temperature in the presence of catalytic amounts (0.05−1 mol %) of $Y_5(O\textit{i}\text{-Pr})_{13}O$ or $Y(thd)_2(\textit{i}\text{-PrO})$ [thd = 2,2,6,6-tetramethyl-3,5-heptanedionato] to give the corresponding esters in quantitative yield (eq 1).[3a] It was later found that the salen complexes[3b,4] of yttrium significantly enhanced the rate of the acyl transfer process as compared to the yttrium alkoxides, enabling these reactions to be carried out at temperatures as low as −25 °C with 1 mol % of the catalyst (Scheme 1). When a chiral secondary alcohol such as

(1) (a) Procopiou, P. A.; Baugh, S. P. D.; Flack, S. S.; Inglis, G. A. *J. Org. Chem.* **1998**, *63*, 2342 and references cited therein. (b) Ishihara, K.; Kubota, M.; Kurihara, H.; Yamamoto, H. *J. Am. Chem. Soc.* **1995**, *117*, 4413. (c) Kawabata, T.; Nagato, M.; Takasu, K.; Fuji, K. *J. Am. Chem. Soc.* **1997**, *119*, 3169. (d) Fu, G. C. *Acc. Chem. Res.* **2000**, *33*, 412. (e) Vedejs, E.; Jure, M. *Angew. Chem., Int. Ed.* **2005**, *44*, 3974. (f) France, S.; Guerin, D. J.; Miller, S. J.; Lectka, T. *Chem. Rev.* **2003**, *103*, 2985. (g) Birman, V. B.; Li, X. *Org. Lett.* **2006**, *8*, 1381 and references cited therein.

(2) (a) Faber, K.; Riva, S. *Synthesis* **1992**, 895. (b) Degueil-Castaing, M.; De Jeso, B.; Drouillard, S.; Maillard, B. *Tetrahedron Lett.* **1987**, *28*, 953. (c) Wang, Y.-F.; Lalonde, J. J.; Momongan, M.; Bergbreiter, D. E.; Wong, C.-H. *J. Am. Chem. Soc.* **1988**, *110*, 7200. (d) Ishii, Y.; Takeno, M.; Kawasaki, Y.; Muromachi, A.; Nishiyama, Y.; Sakaguchi, S. *J. Org. Chem.* **1996**, *61*, 3088. (e) Orita, A.; Mitsutome, A.; Otera, J. *J. Org. Chem.* **1998**, *63*, 2420.

(3) (a) Lin, M.-H.; RajanBabu, T. V. *Org. Lett.* **2000**, *2*, 997. (b) Lin, M.-H.; RajanBabu, T. V. *Org. Lett.* **2002**, *4*, 1607.

(4) For a review of salen complexes of lanthanides, see: Liu, Q.; Meermann, C.; Görlitzer, H. W.; Runte, O.; Herdtweck, E.; Sirsch, P.; Törnroos, K. W.; Anwander, R. *J. Chem. Soc., Dalton Trans.* **2008**, 6170 and references cited therein.

DOI: 10.1021/jo100206d Published on Web 03/11/2010

SCHEME 1. Enhancement of Rate by a Y−Salen Complex and Kinetic Resolution

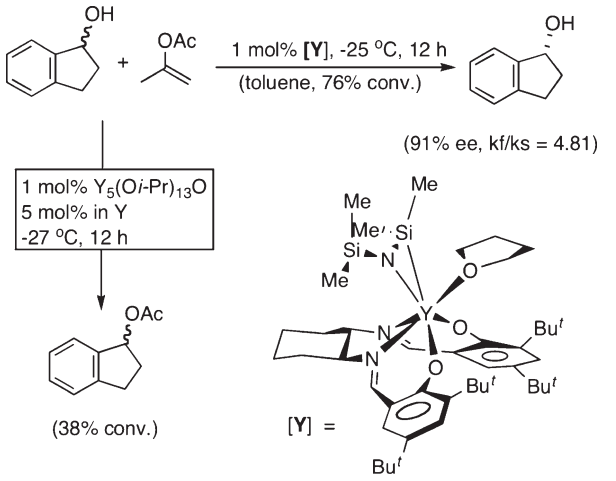

1-indanol was used, moderate enantioselectivity in the acylation was also observed. Thus, at 76% conversion, a kinetic resolution ensued resulting in the accumulation of the less reactive (*R*)-enantiomer in an enantiomeric ratio of 95.5:4.5.

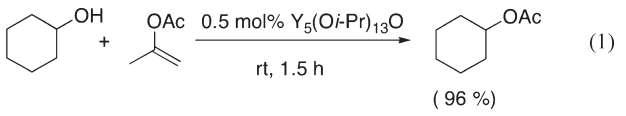

(1)

The catalytic efficiency of the yttrium(III)−salen complex is unique, as many other metal complexes (among them, salen complexes of Sc, lanthanides, Al, Cr, and Mn, as well as pyridine bis-oxazoline and bis-oxazoline complexes of Cu and Sn) showed very little activity.[3b] The mechanism of this remarkable reaction remains to be elucidated; however, as an initial attempt to understand this process, RajanBabu and co-workers have determined the solid-state structure of the yttrium catalyst (Scheme 1, [**Y**]).[3b] The complex incorporates one anionic ligand [$^{-}$N(SiHMe$_2$)$_2$] and one neutral ligand (THF), and notably, this complex has a distorted trigonal prismatic structure rather than the familiar octahedral geometry seen in most transition metal−salen complexes. The large yttrium atom is placed 0.95 Å above the N_2O_2 plane. Replacement of the two ligands by an alkoxide (anionic) and an enol ester (neutral) could lead to activation of both these reactants within the coordination sphere of yttrium. If the intermediate retains the distorted trigonal prismatic structure of the starting complex, the two reacting partners (the "nucleophile" and the "electrophile") are held in close proximity. An internal nucleophilic attack by the alkoxide on the carbonyl group could initiate a cascade of events leading to the final products (Scheme 2). Such a novel mechanism may have validity beyond the acyl transfer process described here, including for applications such as

(5) (a) Dechy-Caberet, O.; Martin-Vaca, B.; Bourissou, D. *Chem. Rev.* **2004**, *104*, 6147. (b) O'Keefe, B. J.; Hillmyer, M. A.; Tolman, W. B. *J. Chem. Soc., Dalton Trans.* **2001**, 2215. (c) McLain, S. J.; Drysdale, N. E. *Polym. Prepr.* (*Am. Chem. Soc., Div. Polym. Chem.*) **1992**, *33* (174), 463. (d) Ovitt, T. M.; Coates, G. W. *J. Am. Chem. Soc.* **2002**, *124*, 1316. (e) Saha, B.; Lin, M.-H.; RajanBabu, T. V *J. Org. Chem.* **2007**, *72*, 8648–8655. (f) Wu, B.; Parquette, J. R.; RajanBabu, T. V. *Angew. Chem., Int. Ed.* **2009**, *48*, 1126–1129. (g) Wu, B.; Parquette, J. R.; RajanBabu, T. V. *Science* **2009**, *326*, 1662.

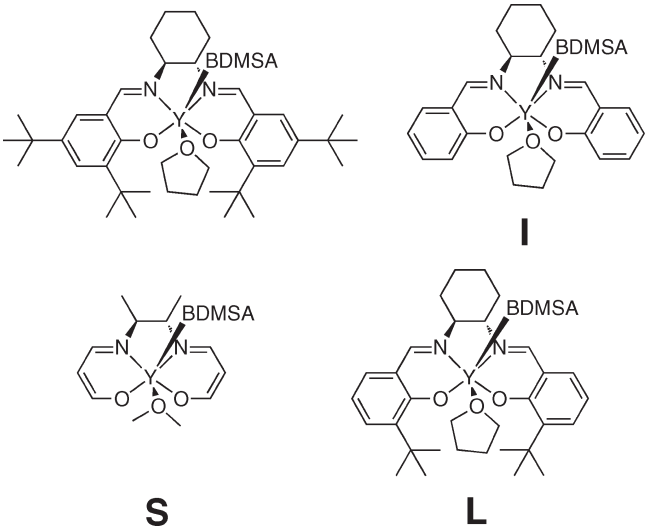

FIGURE 1. Full salen complex (top left) and three truncated models that were employed in this study. The models are classified as initial (**I**), for the model employed in the first reaction surface sampling, small (**S**), used in initial transition state identification, and large (**L**), which reintroduces the *tert*-butyl groups believed to contribute to the selectivity of the catalyst.

SCHEME 2. A Possible Dual Activation of Substrates in Y(III)-Catalyzed Acyl Transfer

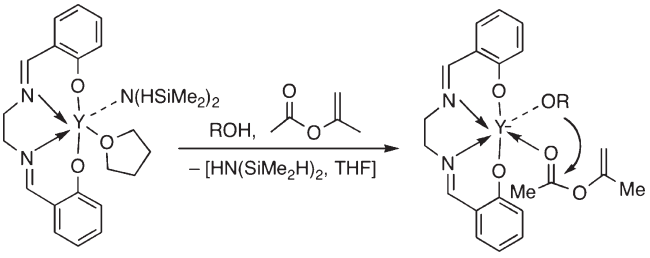

the Y(III) alkoxide initiated polymerization of lactones and lactides.[5a−d] Chiral yttrium−salen complexes have also been found to have broad applications in the enantioselective ring-opening reactions of aziridines and epoxides by silyl azides and cyanides.[5e−g] Accordingly, we embarked on a computational study to examine the veracity of such a mechanism by computational methods, and in this paper, we report the results of this study.

Computational Methods

Model Systems. Three different computational models of the yttrium−salen complex were employed in the course of this study, primarily due to the large size and complexity of the full molecule. The initial model system removed the peripheral *tert*-butyl groups from the salen ligand but kept the rest of the salen intact. A second model was employed for initial transition-state identification and characterization, and this reduced the system size considerably, retaining only the central core of the salen ligand. The final model system restored the *tert*-butyl groups closer to the yttrium (Figure 1). The rationale behind the model choices was the balance between computational efficiency and accuracy, in particular with regard to vibrational frequency analyses, which are critical for transition-state verification. The fragments removed from the model are those which generally do not interact with the ligands above the salen and may

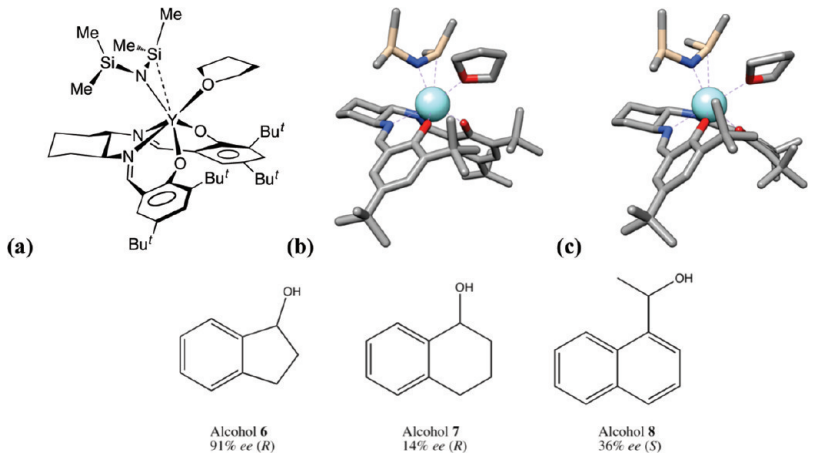

FIGURE 2. Top row: (a) Y−salen complex with bis-dimethylsilylamide, **1**. (b) Crystal structure obtained for complex **1**.[3a] (c) RI-BP86/SV(P), TZVP-optimized structure of complex **1**. Y is shown as a blue sphere. On the bottom row, the three alcohols which were studied, along with the % ee values for the recovered alcohols from experimental studies,[3b] are shown.

be involved in modulating the aggregation state of the complex in solution.

Theoretical Methods. The reaction of alcohols with enolesters catalyzed by the yttrium−salen complexes were modeled using the TURBOMOLE 5.80 and TURBOMOLE 5.91[6−9] suites of programs for electronic structure calculations. Geometry optimizations were performed using the BP86 density functional,[10−13] with the resolution-of-the-identity (RI) approximation (RI-BP86) for simplification of the electronic Coulomb interactions. The TZVP basis set was employed for yttrium, while the SV(P) basis set was used for all other atoms. Single-point energy calculations were performed using the B3LYP hybrid density functional,[14,15] again using the RI approximation (RI-B3LYP). Solvation effects were simulated via single-point energy calculations using RI-B3LYP in conjunction with the COSMO[16] implicit solvation model and a solvent dielectric of 78 to represent a very polar solvent, such as water.

All stationary points on the potential energy surfaces were characterized by vibrational frequency analyses, and minima were verified to have all real vibrational frequencies (except where noted). Transition states were located using the STATPT program in TURBOMOLE and were verified to have a single imaginary vibrational frequency. Transition states were further verified to correctly connect reactants to products via propagation along the imaginary vibrational frequency in both directions, followed by geometry optimization to the respective minima. The freeh module in TURBOMOLE was utilized to calculate thermodynamic corrections to obtain free energies at 298.15 K without scaling. Unless noted otherwise, the energies will be presented as ΔG_{298} in kcal/mol.

The issue of ligand orientations around the transition metal was found to be very important in this study: exchange of position of the non-salen ligands did result in significant changes to the energy of intermediates. To address this, at each point on the reaction potential energy surface, various orientations of the ligand were explored, and the resulting minimum energy conformation was used.

Results and Discussion

Geometry of the Yttrium−Salen Complex. The BP86 density functional, a pure density functional, allows for the use of the RI approximation for the efficient evaluation of Coulombic interactions in electronic structure calculations. The BP86 functional has previously been tested for accuracy in the simulation of fourth-row transition metals, and its performance was found to be comparable to that of more computationally expensive hybrid functionals.[17] In addition, the ability of various functionals to accurately reproduce the geometry of Y complexes has been studied specifically, and the results using the BP86 functional were found to be in good agreement with experimental values.[18] By utilizing the RI-BP86 method, the calculation of large transition-metal complexes is greatly accelerated, a feature which is vital in the study of large transition-metal complexes such as the yttrium salen complexes examined herein.

A crystal structure of the yttrium-salen complex **1** (Figure 2) has been characterized, and its geometric parameters have been determined.[3a] This presents an ideal situation for the calibration of the RI-BP86 method for simulation of yttrium complexes. Accordingly, a series of conformations of the complex were optimized at the RI-BP86/SV(P),TZVP level of theory, and the geometric parameters of the resulting minimum energy conformation obtained were compared with the crystal structure.

Analysis of the optimized geometry shows that the RI-BP86 geometry is very similar to the experimental structure, with deviations in bond distances of less than 0.05 Å (see the Supporting Information for more details). The notable exception is the Si−Y bond distance, corresponding to a dative interaction, which is shorter by 0.16 Å in the crystal structure. Based on the positioning of the bis-dimethylsilylamide (BDMSA) ligand on top of the complex, this bond distance might be more sensitive to crystal packing forces, thus perturbing this bond in the crystal structure. The N−Y−Si bond angle for BDMSA is also slightly smaller, due to the longer bond distance in the computed

(6) (a) Ahlrichs, R.; Bär, M.; Häser, M.; Horn, H.; Kölmel, C. *Chem. Phys. Lett.* **1989**, *62*, 165. (b) For the current version of TURBOMOLE, see http://www.turbomole.de.
(7) Häser, M.; Ahlrichs, R. *J. Comput. Chem.* **1989**, *10*, 104.
(8) Treutler, O.; Ahlrichs, R. *J. Chem. Phys.* **1995**, *102*, 346.
(9) Arnim, M. v.; Ahlrichs, R. *J. Comput. Chem.* **1998**, *19*, 1746.
(10) Slater, J. C. *Phys. Rev.* **1951**, *81*, 385.
(11) Vosko, S. H.; Wilk, L.; Nusair, M. *Can. J. Phys.* **1980**, *58*, 1200.
(12) Becke, A. D. *Phys. Rev. B* **1992**, *45*, 13244.
(13) Perdew, J. P. *Phys. Rev. B* **1986**, *33*, 8822.
(14) Becke, A. D. *J. Chem. Phys.* **1993**, *98*, 5648.
(15) Lee, C.; Yang, W.; Parr, R. G. *Phys. Rev. B* **1998**, *37*, 785.
(16) Klamt, A.; Schürmann, G. *J. Chem. Soc., Perkin Trans. 2* **1993**, 799.
(17) Furche, F.; Perdew, J. P. *J. Chem. Phys.* **2006**, *124*, 044103.
(18) Buzko, V. Y.; Sukhno, I. V.; Buzko, M. B.; Subbotina, J. O. *Int. J. Quantum Chem.* **2006**, *106*, 2236.

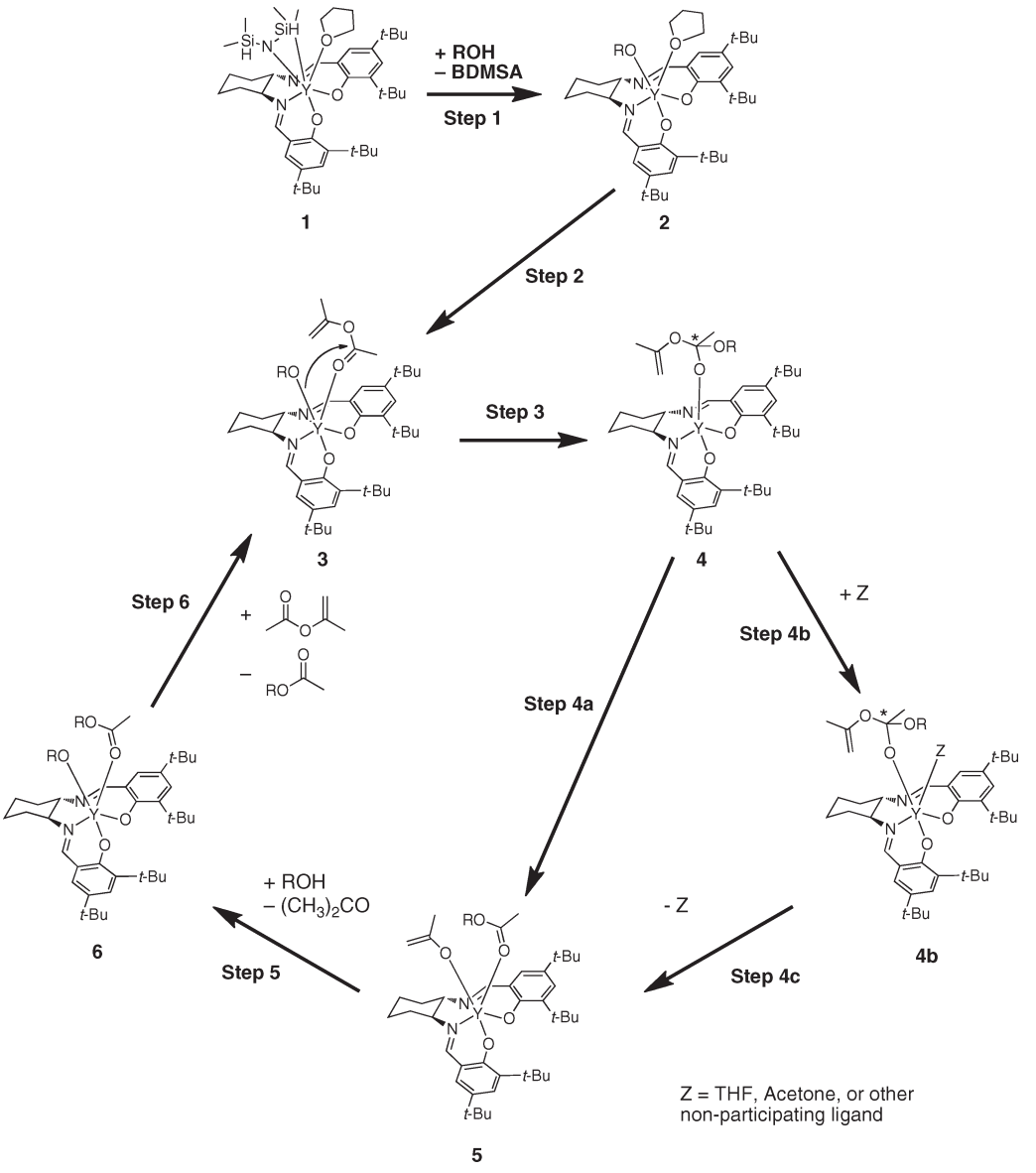

FIGURE 3. Proposed catalytic cycle for the Y-catalyzed acyl transfer reaction of a generic alcohol (ROH). Steps 4b and 4c may involve the association/dissociation of a variety of solvent or other coordinating molecules, in this case THF.

structure. These results may indicate that the density functional method is not modeling the dative interaction precisely; however, this dative interaction is present only in the bis-dimethylsilyl-amide derivative, and the difference in geometry is fairly small.

The yttrium−salen complex itself may exist as either a monomer or dimer, as crystal structures have been resolved for both aggregation states under different conditions. In one crystal structure of the dimer, two hydroxide bridges are shared between the two yttrium atoms, with the salen complexes on opposite sides, and one acetone molecule coordinating to each metal (see the Supporting Information). This is in contrast to the monomeric crystal structure, shown above, which includes the bulky BDMSA ligand as well as a molecule of tetrahydrofuran (THF) coordinating to the metal. In both structures, the salen itself is identical, indicating that the aggregation state of the metal is sensitive to the experimental conditions. A geometry optimization was performed on the dimeric salen complex, as well as on a monomeric model of the complex, with a single water and acetone coordinating to a single Y-salen complex. The energy of the dimeric form of the complex was found to be 16.1 kcal/mol lower in energy than two molecules of the monomer. This value is likely too large to be reasonable and may be the result of a combination of basis set superposition error (BSSE)[19] and the coordination of only six ligands in the monomeric structure owing to the loss of the interaction between the yttrium atoms. The optimized RI-BP86/SV(P),TZVP geometry of the dimer was also highly similar to the crystal structure, with only small deviations in the bond distances for the coordinating residues (see the Supporting Information). With this calibration of the theoretical methods, we proceeded with mechanistic studies on the acyl-transfer process.

Reaction Thermochemistry and Analysis of the Proposed Catalytic Cycle. The postulated mechanism of the yttrium-catalyzed acyl transfer reaction is shown in Figure 3, and we

(19) Kestner, N. R. *J. Chem. Phys.* **1968**, *48*, 252.

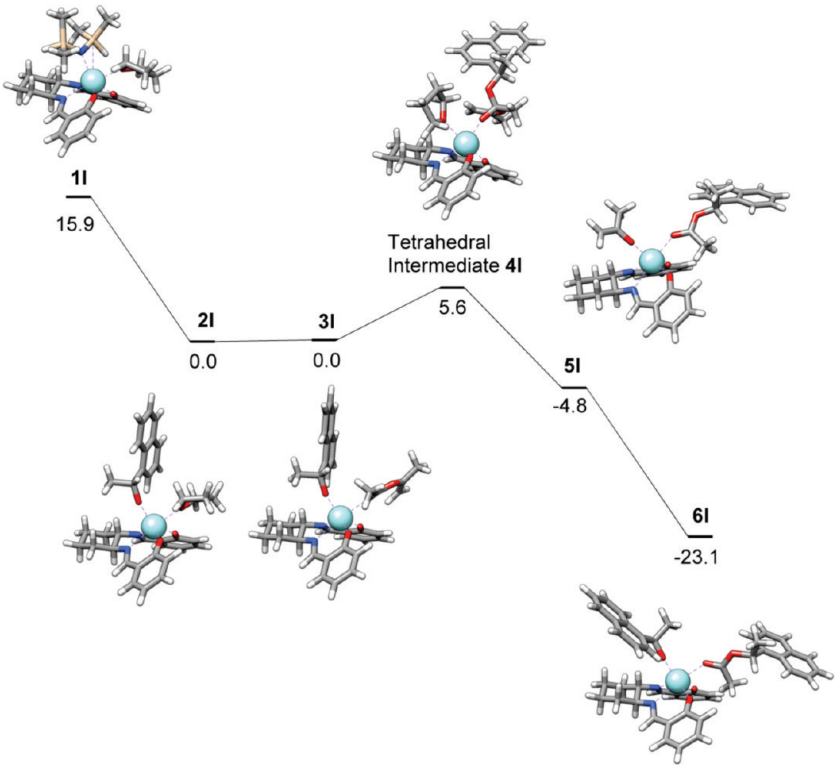

FIGURE 4. Potential energy surface calculated for intermediates in the reaction of 1-(1-naphthyl)ethanol with isopropenyl acetate catalyzed by a truncated yttrium−salen complex. Energies (ΔH_0) are in kcal/mol relative to intermediate **3I**. The transition states between intermediates **3** and **4/5** were not characterized with this model system.

explored this mechanism using computational modeling. Due to the size of the system, initial model studies were performed with the truncated catalyst, both to reduce the computational expense and to reduce the conformational complexity of the system. To that end, the *tert*-butyl groups were removed, leaving the upper surface of the complex significantly less sterically crowded, and reducing the complexity as well. The effect of this modification on the potential energy surface was predicted to be minor, as the groups removed were postulated to be involved primarily in influencing the stereoselectivity of the process, as opposed to actively participating in catalysis. The calculated potential energy surface for the reaction of 1-(1-naphthyl)-ethanol with isopropenyl acetate catalyzed by the truncated model system is shown in Figure 4.

The calculated potential energy surface shows a highly exothermic first step of the reaction, totaling −15.9 kcal/mol, for the dissociation of the bis-dimethylsilylamide ligand and the association of the alcohol substrate to the complex, forming **2I**. This is followed by a nearly isoenergetic ligand-exchange reaction, in which THF is displaced by the enol ester substrate, forming complex **3I**. In the third step of the cycle, intramolecular nucleophilic attack by the alcohol oxygen onto the carbonyl group of the enol ester occurs, forming a tetrahedral intermediate, which can either have a molecule of solvent coordinate to the vacant coordination site transiently (intermediate **4I**) or directly collapse to produce complex **5I**, while the acylated alcohol and the enol of acetone coordinate to the yttrium. The tetrahedral intermediate **4I** is of particular importance, as an additional chiral center is generated on the carbonyl carbon, which means that a total of four diastereomeric transition states are generated with the reaction of a chiral alcohol containing one stereogenic center. Following formation of **5I**, the acylated alcohol has been formed, and the remaining two exothermic steps of the catalytic cycle are ligand exchange of the enolate of acetone for a new alcohol molecule (the enol form of acetone would rapidly tautomerize) and the ligand exchange of the acylated alcohol for a new molecule of enol ester. The final two exchange steps are interchangeable, and other molecules such as solvent could also participate in these exchange reactions, but the described pathway is productive for the catalytic cycle.

The calculated potential energy surface shows a generally isoenergetic or exothermic pathway, aside from a single, moderately endothermic step: formation of the tetrahedral intermediate. This step was proposed to be turnover-limiting by Lin and RajanBabu,[3a,b] and the current findings, in light of Hammond's postulate, appeared to corroborate this idea. To verify this claim, we needed to explicitly calculate the transition states for this process. To simplify the process of transition state characterization, we truncated the model system further, and used a highly simplified alcohol substrate, (*R*)-3-buten-2-ol. This new model (**S** series, Figure 1) lacked most of the peripheral groups but was electronically similar to the initial complex.

To verify that the truncated model was suitable for modeling the reaction, the intermediates along the catalytic cycle were all calculated using the smaller model (**S**, Figure 1) system, and the resulting energies and structures were compared to those found in the larger model; the free energy surface resulting from these calculations is shown in Figure 5.

The reduction in size of the model system and consideration of free energies did not alter the overall shape of the free energy surface for the catalytic cycle, with the process remaining energetically favorable and with formation of the

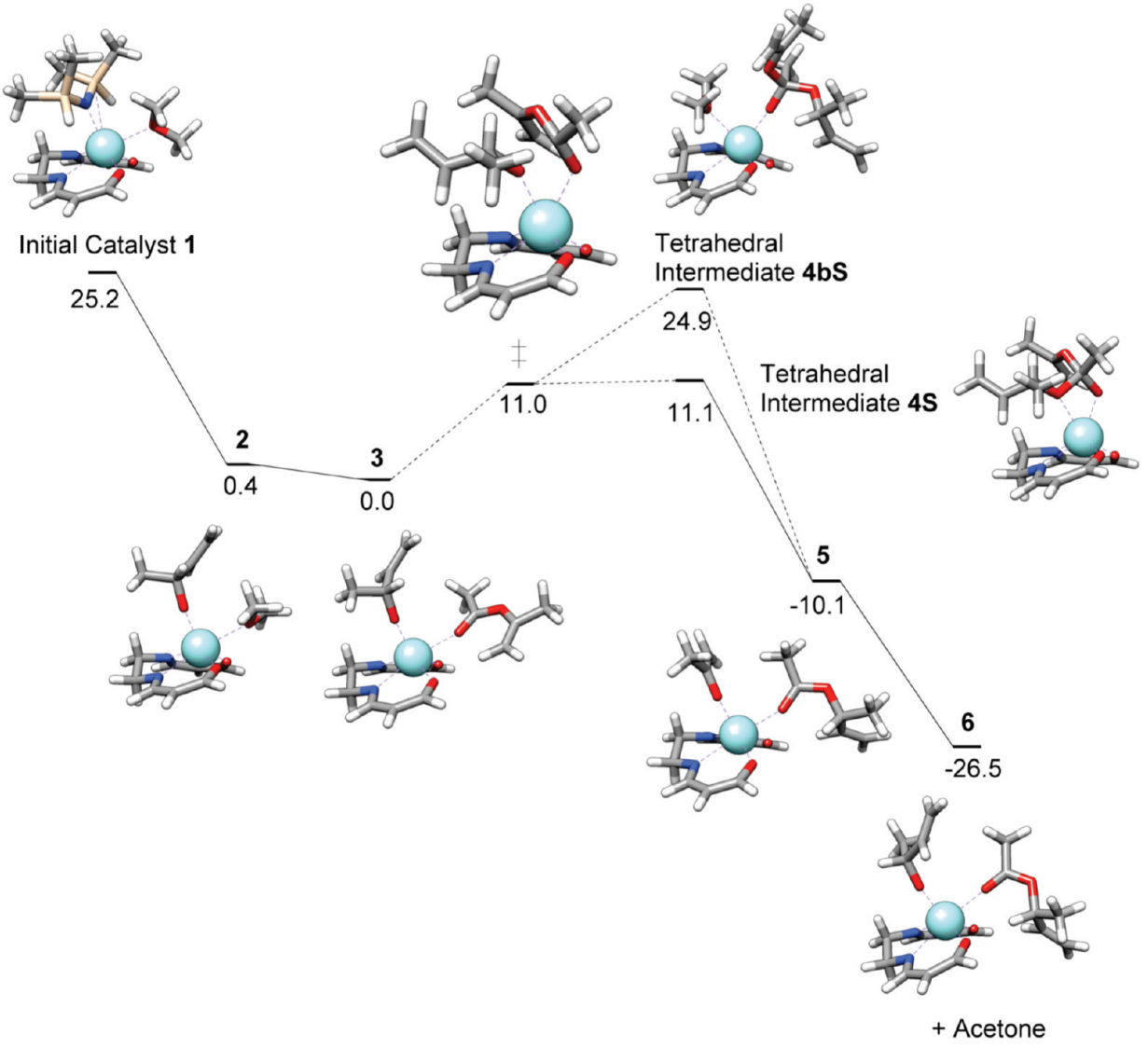

FIGURE 5. Using the **S** model (Figure 1) of the yttrium catalyst, the calculated free energy surface for the reaction of (*R*)-3-buten-2-ol with isopropenyl acetate is shown. The energies shown are ΔG_{298} in kcal/mol for each step in the pathway.

tetrahedral intermediate being the apparent turnover-limiting step for the cycle. However, the alternative reaction pathway involving intermediate **4bS** was considerably higher in energy, owing primarily to the entropic penalty arising from coordination of an additional solvent molecule. *An examination of the geometric parameters of the truncated catalyst **1S** showed that the structure, despite the removal of many of the peripheral groups, remained similar to the larger model system* (*see* the *Supporting Information*). *As such, the smaller model was used for transition state identification and characterization.*

Transition-State Calculations. The stereoselectivity of the acylation reaction originates in the relative heights of the diastereomeric transition states relative to their prereactant complexes. As such, to be able to predict and rationalize the observed stereoselectivities, we needed to identify and characterize the transition state for the putative turnover-limiting step, the intramolecular nucleophilic attack of the alkoxide into the carbonyl of the enol ester (Figure 5).

We began with a relaxed potential energy surface scan along the O−C(=O) coordinate, which identified a maximum at 1.7 Å for the (R)O−C(=O) bond length. Upon refinement, the transition state was identified at a bond distance of 1.83 Å, with a barrier for the reaction of 10.8 kcal/mol, and endothermicity for formation of the tetrahedral intermediate of 10.0 kcal/mol. In the transition state, the yttrium remains hexacoordinate, with both oxygens of the substrate maintaining interactions with the metal and bond distances of 2.30 and 2.28 Å for the alcohol and enol ester, respectively. While subsequent coordination of THF (or other ligands) is possible, and does reduce the enthalpy of the tetrahedral intermediate somewhat (intermediate **4bS**), the congested space above the plane of the salen ligand requires rearrangement of the intermediate, and cleavage of one Y−O bond, before such an association is possible. Further, while it is enthalpically favorable, a large negative entropy associated with the coordination renders the process thermodynamically disfavored, and as a result, it is not likely to contribute to the selectivity of the catalytic cycle. It is noteworthy that the calculated transition state does pose the two reactants in close proximity while maintaining coordination to the yttrium metal, and thus, the calculated geometry

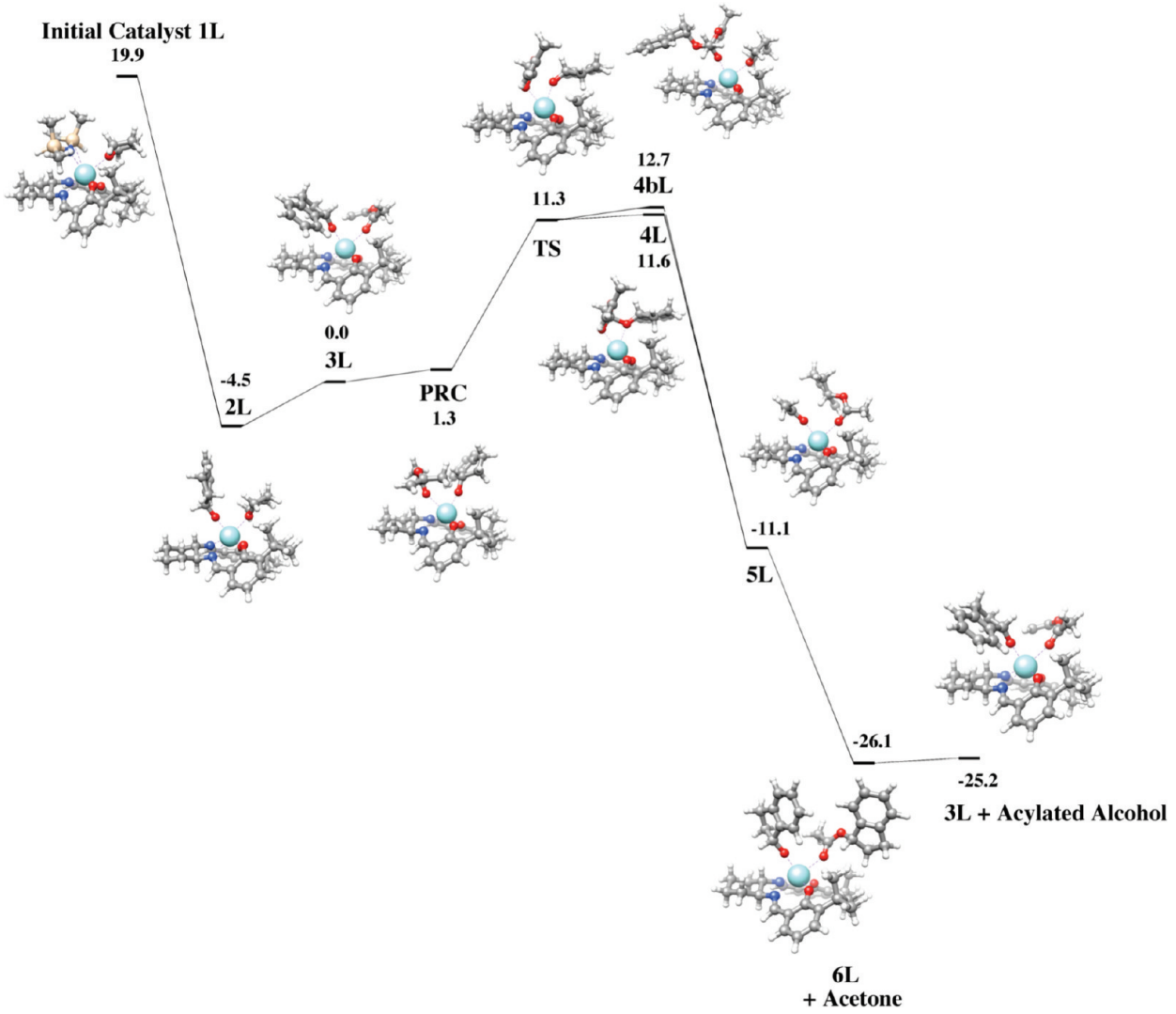

FIGURE 6. Calculated free energy surface for acylation of alcohol **6** via the *S*,*Re* diastereomeric pathway using the large (**L**) model of the catalyst. The geometries and energies were obtained at the BP86/SV(P),TZVP level of theory.

provides some additional rationalization of the proposed reaction mechanism.

Having identified the geometry of the transition state in a smaller model system, we proceeded to attempt characterization of transition states in a larger model system in order to see if the stereoselectivity of the reaction could be rationalized.

Rationalizing the Observed Stereoselectivity. Kinetic resolution of several alcohols by yttrium−salen complexes have been reported experimentally; three alcohols that showed significant reaction selectivities are shown in Figure 2. Of the three, alcohol **6** (1-indanol) showed the largest selectivity, with lesser amounts reported for **7** (1,2,3,4-tetrahydro-1-naphthol) and **8** (1-(1-naphthyl)ethanol). Interestingly, the reaction selectivity for alcohol **8** is reversed, with acylation of the *R* alcohol favored, although the overall enantioselectivities observed for acylation of alcohols **7** and **8** are fairly low. We proceeded to model the free energy surfaces for the acylation reaction, including calculation of the diastereomeric transition states for the intramolecular nucleophilic step characterized above as being the probable turnover-limiting step, to both attempt to rationalize the observed enantioselectivity and to probe the viability of the proposed catalytic cycle.

Alcohol 6. In the reported reaction,[3a,b] kinetic resolution of alcohol **6** was found to give 91% ee with a preference for acylation of the *S* alcohol, with 76% conversion after 12 h at −25 °C. We began with a conformational search of each of the intermediates for one diastereomeric pathway, in order to verify that the qualitative shape of the surface was similar to that studied above. The overall free energy surface for the *S*,*Re* diastereomeric reaction pathway for alcohol **6** is shown in Figure 6. The *S*,*Re* designation corresponds to the *S* stereoisomer of the alcohol and *Re* stereochemistry for the developing tetrahedral intermediate; this nomenclature is preserved for all of the examined alcohols. The free energy surface calculated for the reaction of alcohol **6** is qualitatively quite similar with those described above, again with the tetrahedral intermediate being the highest energy point on the surface (aside from the initial catalyst). Accordingly, the formation of this intermediate was again deemed the probable turnover-limiting step, and transition-state characterization was performed to obtain relative barrier heights for the four diastereomeric transition states.

After verifying that the shape of the free energy surface for the reaction of **6** resembled those studied in the smaller model

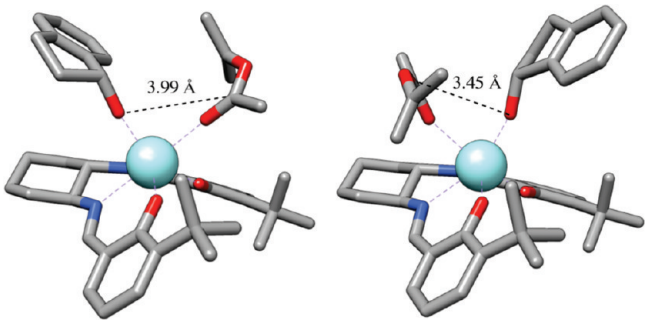

FIGURE 7. Comparison of intermediate **3L** and the connecting prereactant complex identified from the rotational scan of the *R,Re* diastereomer with alcohol **6**. The conformer to the left is lower in energy by 7.9 kcal/mol (ΔG_{298}) but has a longer separation between alcohol and enol ester and leads to a higher energy transition state for formation of the tetrahedral intermediate.

systems, we proceeded to perform a relaxed potential energy surface scan along the coordinate for intramolecular nucleophilic attack for each of the four diastereomeric intermediates. Complicating this study was the identification of two minima for the prereactant complex, corresponding to two orientations of the alcohol and enol ester. In the generally lower energy conformation (designated **3L**), the alcohol is positioned above the cyclohexyl fragment, with the enol ester near the *tert*-butyl groups, while in the alternate conformation, the two units switch positions, with the alcohol bridging the *tert*-butyl groups. The latter conformation was generally found to be higher in energy by up to 8 kcal/mol; however, subsequent transition-state calculations found that the absolute energies of the transition states from that position were lower by ~1 kcal/mol (see the Supporting Information). Accordingly, the conformation leading to the productive transition state has been designated the prereactant complex (PRC). The two intermediates identified for the *R,Re* diastereomer are shown in Figure 7.

Analysis of the transition states predicted for the acylation of **6** found that both the absolute and relative barrier heights for the diastereomers were highly similar (Table 1). Absolute transition-state free energies were within 1.0 kcal/mol for the four diastereomers, with the *S,Re* diastereomer possessing the lowest energy. The *S,Re* diastereomer also possessed the lowest activation barrier, with the transition state being 11.3 kcal/mol above conformation **3L** and 10.0 kcal/mol higher in energy than the connecting prereactant complex. The next lowest transition state barrier was observed for the *S,Si* transition state, which had a barrier of 11.9 kcal/mol from the prereactant complex and 11.8 kcal/mol relative to conformation **3L**. The remaining two transition states, for the *R* alcohol, had overall activation barriers of 14.9 and 15.4 kcal/mol and barriers from the prereactant complex of 7.0 and 9.5 kcal/mol for the *R, Re* and *R,Si* diastereomers, respectively. It should be noted that the energetic preference for acylation of the *S* enantiomer was reproduced from the both the activation barriers and absolute transition state free energies; however, when only reaction enthalpies are considered, the *R,Re* diastereomeric transition state is lowest in energy. This suggests that the conformational entropies are quite important in dictating the overall selectivity of the reactions (*see the Supporting Information for additional details on transition-state geometries*).

To explore whether the choice of density functional or the absence of solvation treatments influenced the predicted reaction selectivities, we performed single-point energy calculations using the B3LYP density functional,[14,15] followed by additional single-point calculations with B3LYP and use of the COSMO implicit solvation model (with a dielectric constant of 78 for water).[16] While the experimental conditions for the acyltransfer reaction were predominantly lower dielectric solvents (e.g., toluene, dielectric constant of 2.4), the COSMO model is most accurate in high dielectric systems, and additionally, the intervening dielectric values can be interpolated as between the values obtained in vacuo and with a dielectric of 78. The results of these calculations are shown in Table 1.

The predicted barrier heights for the turnover-limiting step of the reaction changed by several kcal/mol with the B3LYP functional and by up to 3 kcal/mol when including implicit solvation. A systematic effect of changing to the B3LYP functional was an increase in the transition-state energy relative to both the connecting prereactant complex and conformation **3L**, while inclusion of COSMO solvation differentially stabilized the PRC, resulting in slight (1−2 kcal/mol) increases in the activation barrier for the acylation of the *S* alcohol. The change in density functionals did not significantly alter the predicted reaction selectivities, with a small preference for the experimentally observed *S* acylation retained across the theoretical methods. *It should be noted that transition states characterized for S,Re acylation were consistently the lowest in absolute energy (albeit by a small amount) for both functionals, while the inclusion of COSMO solvation resulted in a small preference for the R,Si transition states. In the latter case, however, the activation energy relative to the lowest energy reactant conformation remains more favorable for the S,Re pathway. As with the BP86 results above, the consideration of enthalpy alone did not support the observed reaction selectivities, with the R,Si diastereomeric transition state 1 kcal/mol lower in absolute enthalpy than that for the S,Re pathway.*

One possible complicating factor in simulating this reaction could be the participation of a dimeric or potentially higher

TABLE 1. Calculated Reaction Barriers for the Intramolecular Nucleophilic Attack of Alcohol 6 Using the L Model of the Yttrium Catalyst and Relative Transition State Energies[a]

Alcohol **6**	BP86//BP86			B3LYP//BP86			B3LYP(COSMO)//BP86		
diastereomer	**3L**	**PRC**	**TS**	**3L**	**PRC**	**TS**	**3L**	**PRC**	**TS**
R,Re	14.9	7.0	1.0	17.2	9.0	0.9	17.5	11.7	0.9
R,Si	15.4	9.5	1.0	17.3	11.2	0.6	16.7	12.5	0.0
S,Re	11.3	10.0	0.0	13.4	11.9	0.0	13.9	14.1	0.2
S,Si	11.8	11.9	0.2	14.0	13.8	0.1	14.3	16.1	0.3

[a]Barriers were calculated both from the minimum energy prereactant complex conformation **3L**, as well as the prereactant complex (PRC) obtained following propagation of the transition state (TS) vector toward reactants. All ΔG_{298} values are in kcal/mol. The SV(P),TZVP basis set was used in each case. See Figure 4 for a representative free energy surface and for designations.

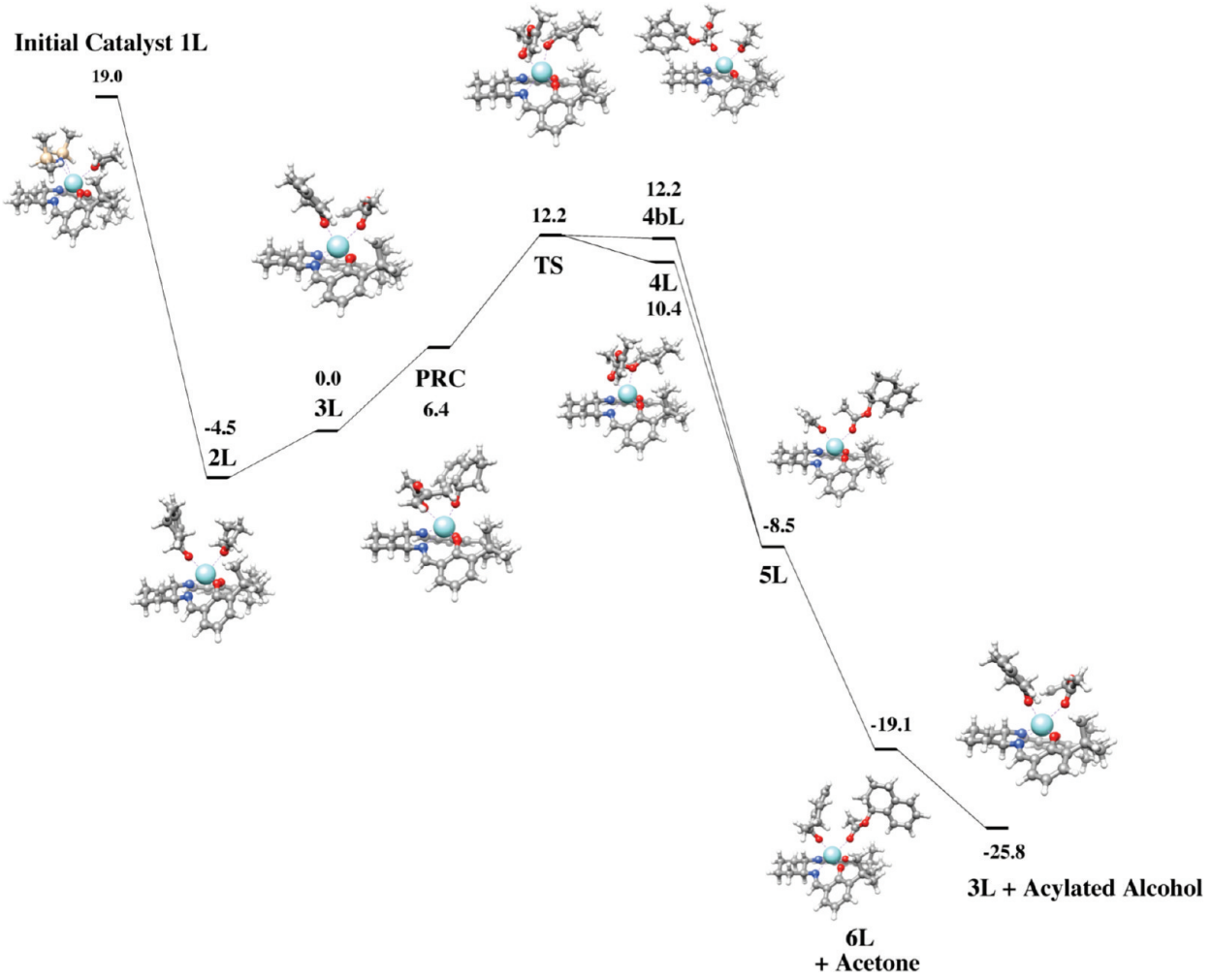

FIGURE 8. Calculated free energy surface for acylation of alcohol **7** via an *S*,*Re* diastereomeric pathway in the large (**L**) model of the yttrium−salen complex. The geometries and energies were calculated at the RI-BP86/SV(P),TZVP level of theory. The transition-state barrier for the *S*,*Re* diastereomer was 12.2 kcal/mol (ΔG_{298}) relative to the lowest energy prereactant complex. For the *R*,*Re*, *R*,*Si*, and *S*,*Si* diastereomers, the barriers were 17.9, 17.4, and 15.3 kcal/mol, respectively.

order yttrium complex, despite the monomeric nature of the starting catalyst; such a species could potentially compete with the monomeric catalyst, and the predicted selectivities would not necessarily be the same. The reaction free energy surface is also quite complex, and the association of other species during the formation of the tetrahedral intermediate could influence the reaction, potentially stabilizing the intermediate and altering the kinetics of product formation. This was considered via the association of a molecule of THF to the tetrahedral intermediate formed after the putative turnover-limiting step (intermediate **4bL**, in Figure 6). In a similar fashion to the small model results, above, this intermediate was lower in enthalpy by 5−7 kcal/mol but had a significant entropic penalty that resulted in it being roughly isoergic (±3 kcal/mol) with the various diastereomeric transition states. This result suggests that intermediate **4bL** is unlikely to connect to a lower energy transition state than the main reaction pathway. Having successfully predicted the experimental selectivities (albeit by a small margin), we next performed similar modeling studies on alcohols **7** and **8** to further examine our ability to predict the experimental selectivities.

Alcohol 7. Modeling of the reaction of alcohol **7** with the **L** model of the salen complex (Figure 1) was also performed. The experimental enantiomeric excess was 14%, with acylation of the *S* alcohol preferred. With the significantly lower reaction selectivity, it was expected that the diastereomeric transition states would be closer in energy, although the absolute magnitude of the transition-state barrier was expected to be higher; the experimental conditions suggested that acylation of alcohol **6** was more facile, as the reaction progressed to 76% conversion at −25 °C after 12 h, as compared with 39% conversion at −10 °C after 8 h for alcohol **7**. Similar potential energy surface scans on the alcohol **7**−salen complex were performed, including a 360° rotational scan along the surface of the alcohol to sample the orientation of the prereactant complex above the salen complex (see the Supporting Information).

The reaction profile for alcohol **7** was found to be qualitatively similar to that for alcohol **6**, with initial dissociation of the bis-dimethylsilylamide found to be highly favorable and the intramolecular nucleophilic attack predicted to be turnover-limiting (Figure 8). From the minimum energy conformation of the prereactant complex **3L**, the overall change in free energy over the cycle was found to be −26 to −28 kcal/mol for the four diastereomeric pathways. The ligand exchange reaction to

TABLE 2. Calculated Reaction Barriers for the Intramolecular Nucleophilic Attack of Alcohol 7 Using the L Model of the Yttrium Catalyst and Relative Transition State Energies[a]

alcohol **7**	BP86//BP86			B3LYP//BP86			B3LYP(COSMO)//BP86		
diastereomer	**3L**	**PRC**	**TS**	**3L**	**PRC**	**TS**	**3L**	**PRC**	**TS**
R,*Re*	17.4	11.9	3.8	20.1	14.1	4.2	17.7	15.4	2.0
R,*Si*	17.9	12.6	3.6	20.2	15.0	3.5	19.6	16.2	3.0
S,*Re*	12.2	5.8	0.0	14.5	7.8	0.0	15.1	10.3	0.0
S,*Si*	15.3	9.0	0.6	17.4	11.2	0.3	17.4	13.6	0.3

[a]Barriers were calculated both from the minimum energy prereactant complex conformation **3L** as well as the prereactant complex (PRC) obtained following propagation of the transition state (TS) vector toward reactants. All ΔG_{298} values are in kcal/mol. The SV(P),TZVP basis set was used in each case. See Figure 5 for a representative free energy surface and for designations.

substitute the enol ster for a molecule of THF was slightly exothermic, similar to that for alcohol **6**. In addition, the predicted barrier height is significantly higher than that for alcohol **6**, with overall barriers from **3L** being higher by between 1−4 kcal/mol. As the experimental rate of reaction for alcohol **7** was slower (thus, the reaction was performed at a higher temperature), a higher predicted barrier for the reaction is consistent with experiment. Aside from these differences, the overall reaction pathway was quite comparable, including the presence of two discrete conformations of the prereactant complex (PRC). As was seen with alcohol **6**, the orientation of the PRC with the alcohol positioned above the cyclohexyl fragment was lower in energy, while the transition state obtained from the complex with the alcohol above the *tert*-butyl groups was lower in energy (see the Supporting Information). The free energy surface calculated for the *S*,*Re* diastereomeric pathway is shown in Figure 8, and similar free energy surfaces for the other diastereomers are provided in the Supporting Information.

The predicted reaction selectivity for the acylation of alcohol **7** is consistent with experiment, with a preference for acylation of the *S* alcohol being predicted at this level of theory (Table 2).

In contrast to the case of alcohol **6**, there are significantly larger differences in the absolute energies of the transition states calculated for alcohol **7**, which contribute to the predicted reaction selectivity. Using the BP86 functional, the *S*,*Re* transition state is 3.6 and 3.8 kcal/mol lower in energy than that the *R*,*Si* and *R*,*Re* transition states, respectively, while the energy difference is 3.5 and 4.2 kcal/mol at the B3LYP//BP86 level of theory. The *S*,*Si* transition state is 0.6 and 0.3 kcal/mol higher in energy, as calculated using BP86 and B3LYP. In addition, the predicted reaction barriers similarly favor acylation of the *S* alcohol, via the *S*,*Re* pathway, relative to both the lowest energy conformation **3L** and the connecting prereactant complex. Geometric parameters from the transition states calculated for alcohol **7** are available in the Supporting Information. In general, the geometries of the transition states were quite comparable between diastereomers, with bond distances rarely deviating more than 0.02 Å. The N−C−C−N dihedral angle, comprising the backbone of the salen ligand, also did not vary significantly, showing changes of less than 1° between the four diastereomeric transition states. The principal difference between the transition states is the orientation of the alcohols over the salen moiety. For the *S* configuration alcohols, the cyclohexyl portion, as well as the alcohol moiety itself, is positioned in between the two *tert*-butyl groups of the salen. In contrast, for the *R* configuration alcohols, the cyclohexyl portion and alcohol are on the outside of the *tert*-butyl group, with the benzyl portion in between (Figure 9).

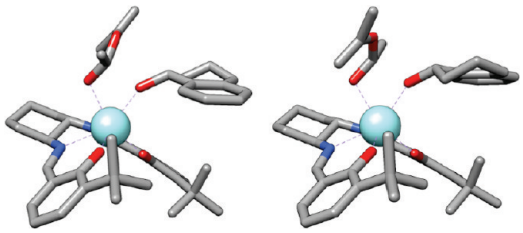

FIGURE 9. *R*,*Si* (left) and *S*,*Re* (right) transition states for the acylation of alcohol **7** optimized at the BP86/SV(P),TZVP level of theory. The *S*,*Re* transition state is 3.6 kcal/mol lower in energy (ΔG_{298}).

The difference in transition-state energies could thus be a result of the van der Waals interactions between the *t*-butyl groups and the rings of the alcohol. Overall, the predicted selectivity for the acyl transfer reaction of alcohol **7** is consistent with experiment, although in contrast to alcohol **6**, the computational selectivity appears to exceed the experimental selectivity. The predicted barriers for the turnover-limiting step were also higher in energy than those observed for alcohol **6**, which is consistent with the slower observed rate of reaction for **7**. We proceeded to examine the reaction of the final compound, alcohol **8**.

Alcohol 8. Calculations were also performed to model the acylation reaction of alcohol **8**. Experimentally, this reaction proceeded with 36% ee for *R* acylation (based upon recovery of unconverted *S* alcohol) under kinetically controlled conditions at −3 °C, with 61% conversion after 7.5 h, a reversal of the selectivities observed for alcohols **6** and **7**. We hoped to reproduce this difference as additional validation of the reaction pathway. The calculated free energy surface for the reaction of the *R*,*Si* isomer is shown in Figure 10, and the predicted reaction barriers for the diastereomeric transition states at the different levels of theory are given in Table 3.

The predicted free energy surfaces for the acylation of alcohol **8** are qualitatively similar, and particularly for the two lowest energy pathways, leading to the *R*,*Si* and *S*,*Re* diastereomeric transition states. For these two pathways, both the absolute free energies of the two transition states and the transition-state barrier heights were within 1 kcal/mol for the gas-phase simulations, although this increased slightly with COSMO solvation. The *R*,*Si* transition state was lowest in absolute energy using both BP86 and B3LYP (and isoenergetic using the TPSS functional, see the Supporting Information); in the gas phase, however, the activation barrier for *S* acylation via the *S*,*Re* transition state from intermediate **3L** was slightly lower in energy, albeit by less

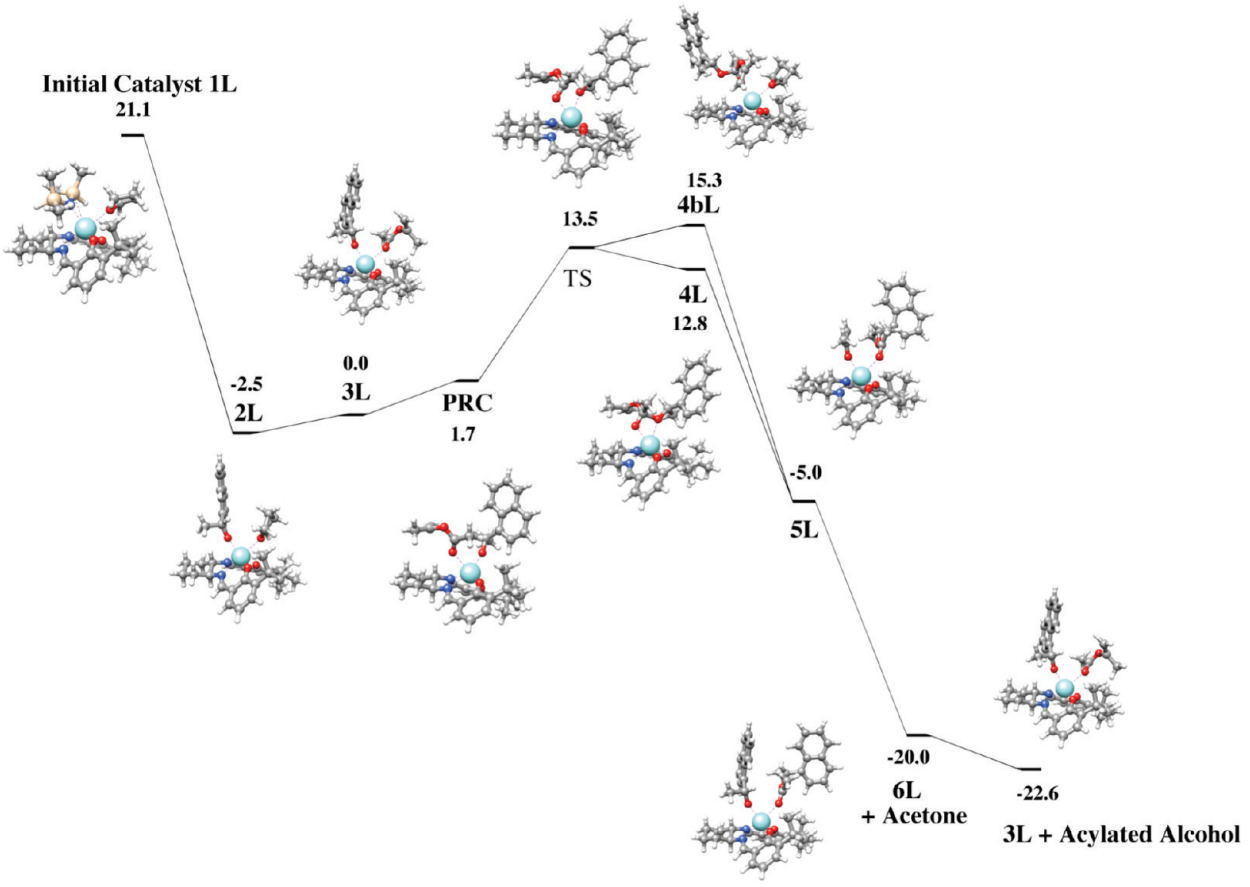

FIGURE 10. Free energy surface for the acylation of the *R*,*Si* enantiomer of alcohol **8** calculated using the large (**L**) model of the yttrium catalyst (RI-BP86/SV(P),TZVP). Energies (ΔG_{298}) are in kcal/mol relative to the minimum energy prereactant complex **3L**. Transition-state barriers for the other diastereomers were 17.0, 20.1, and 13.1 kcal/mol for the *R*,*Re*, *S*,*Si*, and *S*,*Re* diastereomers, respectively.

TABLE 3. Calculated Reaction Barriers for the Intramolecular Nucleophilic Attack of Alcohol 8 Using the L Model of the Yttrium Catalyst and Relative Transition State Energies[a]

alcohol **8**	BP86//BP86			B3LYP//BP86			B3LYP(COSMO)//BP86		
diastereomer	**3L**	**PRC**	**TS**	**3L**	**PRC**	**TS**	**3L**	**PRC**	**TS**
R,*Re*	17.0	10.7	3.6	19.2	12.8	3.8	19.1	15.1	4.6
R,*Si*	13.5	11.9	0.0	15.7	13.8	0.0	14.6	14.7	0.0
S,*Re*	13.1	12.1	0.6	15.6	14.1	0.8	16.2	16.1	2.2
S,*Si*	20.1	14.2	1.5	21.6	16.0	1.4	21.9	17.2	2.0

[a]Barriers were calculated both from the minimum energy prereactant complex conformation **3L** as well as the prereactant complex (PRC) obtained following propagation of the transition state (TS) vector toward reactants. All ΔG_{298} values are in kcal/mol. The SV(P),TZVP basis set was used in each case. See Figure 5 for a representative free energy surface and for designations.

than 0.5 kcal/mol. This preference was reversed to favor the *R*,*Si* pathwaywith implicit solvation.

Examination of the transition-state geometries shows that they are quite similar to those found above for alcohols **6** and **7**, with orientations of the alcohol bridging over one of the *tert*-butyl groups. However, the additional methyl group off of the naphthyl ring significantly alters the orientation of the alcohol in the transition state (and PRC). Rather than being approximately parallel to the surface of the salen ligand, the naphthyl ring adopts a perpendicular orientation, in order to avoid unfavorable steric interactions between the methyl substituent on the alcohol and the *tert*-butyl groups on the salen (Figure 11). Geometric parameters for the transition states are available in the Supporting Information.

The orientation of the alcohol is similar for the *R*,*Si* and *R*,*Re* diastereomeric transition states, with the naphthyl group positioned between the two *tert*-butyl groups. The orientation of the enol ester is reversed between the two, with the *R*,*Re* diastereomer positioning the bulkier enol fragment on the same side as the naphthyl fragment of the alcohol and in proximity to the upper *tert*-butyl group. This increased steric congestion results in an increase in energy for both the intermediate conformation **3L** and the prereactant complex of ~4 kcal/mol, as well as an increase in the transition-state energy (where the alcohol and enol ester are brought into closer proximity) of 3.5−4.6 kcal/mol. The transition states for acylation of the *S* alcohol orient the naphthyl ring on the outside of the *tert*-butyl groups, with the methyl group of the alcohol positioned between them. For the *S*,*Si* diastereomer

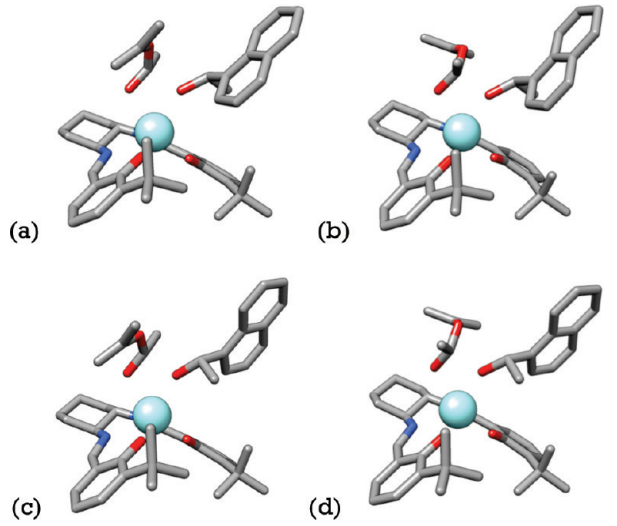

FIGURE 11. Transition states for (a) *R*,*Re*, (b) *R*,*Si*, (c) *S*,*Re*, and (d) *S*,*Si* acylation of alcohol **8** calculated using the RI-BP86/SV(P), TZVP level of theory. The *R*,*Si* and *S*,*Re* transition states had the lowest energies due to the orientation of the bulkier substituents on the alcohol and enol ester to opposite sides of the transition state.

the energy penalty is smaller, despite a similar mismatch to the *R*,*Re* diastereomer, because the enol ester and naphthyl ring are outside of the *tert*-butyl groups, reducing the congestion of the transition state.

While the *S*,*Re* pathway has energetics similar to the *R*,*Si* pathway, the *S*,*Re* process places the naphthyl group outside the *tert*-butyl groups. This orientation is similar to that predicted for the higher energy *R*,*Si* transition state for alcohols **6** and **7**; that is, the bulkier substituent on the alcohol is outside the *tert*-butyl groups. The reverse is seen for the *R*,*Si* transition state for alcohol **8**, as it places the bulkier naphthyl fragment in a similar manner as the lower energy, *S*,*Re* transition states for alcohols **6** and **7**. This trend reflects the experimental selectivities, as alcohols **6** and **7** demonstrated preferential acylation of the *S* alcohol and for **8** the preference was for *R* acylation, and suggests that this orientation of alcohols in the salen complex, with the bulkier substituent bridging the two *tert*-butyl groups, may be operative in the catalytic cycle.

Conclusions

Overall, the free energy surface of a proposed mechanism for the acylation of alcohols with enol esters, catalyzed by a yttrium−salen complex, has been explored using density functional theory methods. This mechanism is of interest because it validates a novel intramolecular acyl transfer step involving nucleophilic attack between two transition-metal-coordinated ligands, with possible implications for the mechanism of lanthanide-catalyzed polymerization of lactides and lactones. The BP86 and B3LYP density functionals were used in the computational modeling for the entire surface, and these methods were found to be in good agreement with only small variations in the predicted reaction barriers. The TPSS density functional, designed in part to improve the treatment of van der Waals interactions, was also employed for the selectivity-determining steps of the reaction surfaces and did not substantially alter the predicted stereoselectivities (see the Supporting Information). This suggests that the more computationally efficient BP86 pure density functional is suitable for simulation of such transition metal complexes; this result has been noted elsewhere as well.[20]

The predicted reaction free energies suggest that the proposed mechanism is a plausible pathway, with accessible energetic barriers and a strong thermodynamic driving force. The putative turnover-limiting step was found to be the most endothermic step in the reaction pathway, and transition-state calculations were successful in identifying and characterizing the transition states both for a small model system and a more robust system including chirally significant groups. However, while the overall shape of the surfaces appeared to be consistent with experiment, including the relative rates of reaction of different substrates, attempts to use theoretical methods to rationalize the observed reaction stereoselectivity led to mixed results.

The absolute transition-state free energies characterized for all three alcohols favored acylation of the correct stereoisomer to match experiment, both in the gas phase and in solution as modeled using the COSMO implicit solvation method. The difference in energies was generally small, with only 0.6−1 kcal/mol favoring the lowest energy transition state for acylation of the *S* enantiomer of alcohol **6** over the corresponding transition states for the *R* enantiomer, which is not as substantial as would be expected given the 91% ee observed. For alcohol **7**, despite having a marginally lower experimental preference for acylation of the *S* alcohol (14% ee), the *S*,*Re* transition state was lower in energy by 2−4 kcal/mol for all methods employed. In addition, for alcohol **8**, which had a reversed preference for acylation of the *R* alcohol with 36% ee, the predicted transition state energies properly reproduced the experimental trend, with the *R*,*Si* diastereomeric transition state lowest in energy by between 0.6 and 2.2 kcal/mol. Overall, the absolute transition state free energies for all three alcohols did properly reproduce the stereochemical trends observed experimentally, with the sole exception being alcohol **6** when calculated using COSMO solvation, which shifted to favor the incorrect acylation product by 0.2 kcal/mol. However, it should be noted that this result was not maintained when the absolute transition state enthalpies were considered alone; for alcohol **6** the incorrect *R* acylation pathway had the lowest enthalpy, and reproduction of the experimental selectivity occurs as the result of a favorable transition state entropy for acylation of the *S* alcohol.

With that said, the orientation of the alcohols in the diastereomeric transition states suggest a possible factor contributing to the experimental selectivities: Placement of the bulkier substituent of the alcohol between the *tert*-butyl groups on the salen complex was predicted for the lowest energy, *S*,*Re* diastereomeric transition states for alcohols **6** and **7**, while the preference was flipped to the *R*,*Si* diastereomer for alcohol **8**, as the methyl substituent on this alcohol forced a rotation of the ligand to place the naphthyl ring perpendicular to the salen core. The absolute transition state free energies correlate well with this observation, and the trend is both consistent with the experimental selectivities for the three alcohols and supported by the known importance of the *tert*-butyl groups in the selectivity of the acylation

(20) East, A. L. L.; Berner, G. M.; Morcom, A. D.; Mihichuk, L. *J. Chem. Theory. Comput.* **2008**, *4*, 1274.

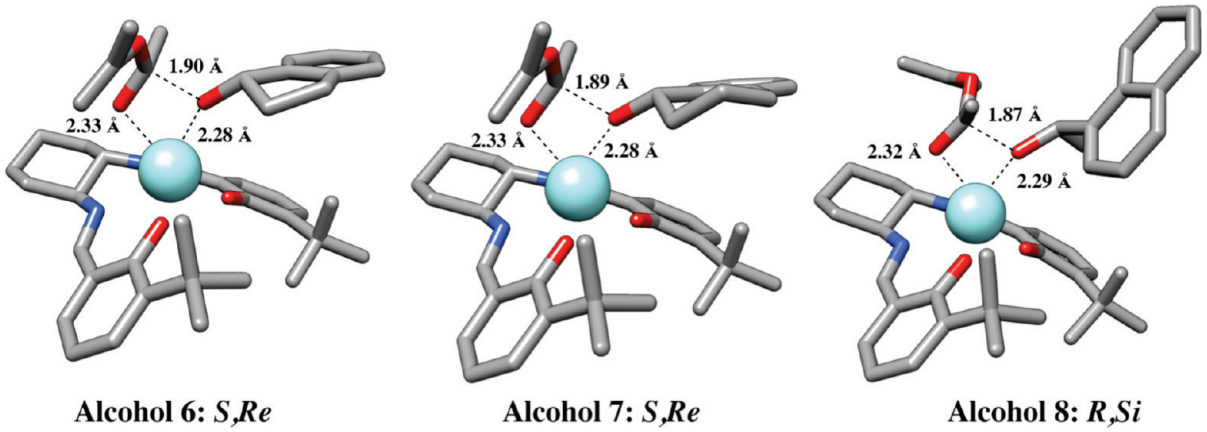

FIGURE 12. Three minimum energy diasteromeric transition states for the intramolecular nucleophilic attack for alcohols **6**−**8**. The *R,Si* and *S,Re* pathways minimize steric interactions between the alcohol and enol ester, with the interactions between alcohol and the salen complex dictating the preference between the two.

reaction. In conjunction with the observation that the *R,Si* and *S,Re* transition states were systematically lowest in energy across all theoretical methods with the three alcohols, we propose that the primary selectivity-determining factor in the turnover-limiting step of the reaction is the reduction in steric clash between the enolester and alcohol as the reaction progresses, bracketed by the salen complex (Figure 12).

The COSMO implicit solvation method was used to examine whether solvation effects might influence the shapes of the reaction free energy surfaces; however, no significant differences were observed upon inclusion of implicit solvation with a dielectric of 78, and the results did not significantly alter the predicted reaction selectivities. Several additional factors which may influence the reaction selectivity have been considered: There may be competition from dimeric metal complexes in solution, which were not examined in this work, or there may be a more complicated series of ligand-exchange and rearrangement steps taking place than were considered herein. The high entropic penalty associated with coordination of an additional ligand to the tetrahedral intermediate, coupled with the high amount of congestion in the salen complex following the coordination of both the alcohol and enolester (e.g., intermediate **3**) does not support such possibilities in a monomeric Y-salen complex as studied herein.

Overall, while not a perfect rationalization of the experimental enantioselectivities, in particular with regard to the magnitudes of enantiomeric excess observed, important observations were made from the computational study. These include validation that the proposed reaction pathway is energetically viable, and that the chiral environment provided by the salen ligand is able to provide significant energetic differences in the relative transition states for the intramolecular nucleophilic attack step, which was identified as being the probable turnover-limiting step. The demonstrated ability of the yttrium salen complex to simultaneously coordinate the alcohol and enolester, and the organization of the two ligands in a productive mode for intramolecular attack also supports the proposed reaction mechanism, which will provide guidance for future studies, in particular for the lanthanide-catalyzed polymerization of lactides and lactones. In addition, the relatively flat energy profile for rotation around the salen complex suggests that equilibration of ligand orientations is relatively facile, conditions under which Curtin−Hammett reaction kinetics could be prevailing. As a result, the absolute transition state energies are likely of primary importance in determining the selectivity of the acylation pathway. This supports the development of a predictive model based primarily on the characterization of diastereomeric transition states for intramolecular nucleophilic attack.

Acknowledgment. Financial support of this work was provided by a National Science Foundation Collaborative Research in Chemistry grant (CHE-0526864). Generous computational resources were provided by the Ohio Supercomputer Center.

Supporting Information Available: Geometric parameters and additional free energy surfaces are included. This material is available free of charge via the Internet at http://pubs.acs.org.